Journal of Physics D:
Applied Physics

PERSPECTIVE

Rate-potential decoupling: a biophysical perspective of electrocatalysis

To cite this article: Peter Agbo 2024 *J. Phys. D: Appl. Phys.* **57** 462001

IOP Publishing

Journal of Physics D: Applied Physics

J. Phys. D: Appl. Phys. **57** (2024) 462001 (12pp)

https://doi.org/10.1088/1361-6463/ad6008

Perspective

Rate-potential decoupling: a biophysical perspective of electrocatalysis

Peter Agbo[1,2,3]

[1] *Chemical Sciences Division, Lawrence Berkeley National Laboratory, Berkeley, CA 94720, United States of America*

[2] *Liquid Sunlight Alliance, Berkeley, Lawrence Berkeley National Laboratory, CA 94720, United States of America*

[3] *Molecular Biophysics & Integrated Bioimaging Division, Lawrence Berkeley National Laboratory, Berkeley, CA 94720, United States of America*

E-mail: pagbo@lbl.gov

Abstract

In this perspective, the chemical physics of biological electron transfer are considered in relation to artificial electrocatalyst development. Nature's ability to access a wide range of chemical reactivities through a relatively narrow set of redox-active motifs, in part by decoupling electron transport rates from reaction driving forces, are suggested as a model for the future of electrocatalyst design and testing. Theoretical rationale and experimental precedents for this concept are put forth, outlining how emulating nature's ability to arbitrarily tune tunneling currents with respect to donor/acceptor redox potentials – reaction driving forces – may enhance our control over electrocatalyst selectivity.

Keywords: electrocatalysis, decoupling, bioinorganic, solar fuels, photoelectrochemistry, artificial photosynthesis, semiconductor-liquid junction

1. Canonical bioinorganic catalysis: the assumed centrality of structure-function relationships

Organometallic mimics of enzyme active sites, such as those of cytochrome P450 porphyrin centers and the oxygen evolving complex (OEC) of photosystem II, have substantially advanced our understanding of their underlying chemical mechanisms and spectroscopic features [1–3]. However, functional mimicry of redox enzymes, particularly through the use of organometallic complexes, has proven uniquely challenging to the field of bioinorganic chemistry. Attempts to link inorganic catalysis and enzyme biochemistry have generally focused on the development of homogeneous molecular catalysts, which act as structural mimics of biological active sites but typically ignore the higher-order aspects of protein design, particularly the roles played by secondary and tertiary structure [4, 5], solvent exclusion effects and regulated electron transport in enzyme catalysis [6, 7]. By and large, synthetic chemists have operated under an implicit assumption that structural mimicry of enzyme active sites should correspond to functional emulation of enzyme catalysis. However, this first approximation has often been found to be necessary but by itself insufficient, with molecular catalysts that superficially resemble protein active centers often failing to replicate enzyme reactivities.

While structure plays a critical role in facilitating enzyme catalysis, this clearly marks only one essential aspect of functional biomimicry. For example, while detailed molecular mimics of photosystem II's OEC have generally failed to fully reproduce the water oxidation chemistry it catalyzes, purely inorganic Mn oxide powders have been found to drive efficient water oxidation [8]. In the specific case of calcium-containing birnessite-like Mn oxides, these materials contain $CaMn_3O_4$ domains similar to the $CaMn_4O_5$ cubanes constituting the OEC, despite omitting the surrounding ligand framework present in both the OEC and organometallic model complexes [1, 8, 9]. The comparative success of inorganic powders (bearing little resemblance to protein active sites) relative to molecular catalyst active site mimics, signal that structural emulation alone is insufficient

for achieving functional mimicry of enzymes. Instead, mastering enzymatic biomimicry at a molecular level will ultimately require that the catalysts being developed—whether homogeneous or heterogeneous—are able to reproduce the underlying physics of the system we are seeking to replicate. In proteins, this requirement encapsulates a broad set of biophysical design components, including the regulation of charge transfer kinetics, the focus of this paper. In particular, this article focuses on the concept of decoupling current density (J) and potential (V) in electrocatalysis as a method for independently controlling charge transport kinetics and energetics in electrocatalysis. Exploration of this subject is motivated by the potential for increased control over carrier dynamics to facilitate more sophisticated characterization of artificial electrocatalysts, while introducing routes for improved control over product selectivities in photoelectrochemical (PEC) systems.

2. Current-potential decoupling and its correspondence with biological electron transfer

The physical possibility of electrochemically decoupling current and potential is suggested by considering electron transfer in biochemical systems, where the decoupling of kinetics and energetics is indeed a physical reality for electronic carriers. In enzymes, the difference in redox potential ($\Delta\varepsilon^0$) between a donor (D) and acceptor (A) site dictates the magnitude of the electrical potential through which an electron is transferred. Systems featuring strong couplings between donor and acceptor states are termed adiabatic; weakly-coupled electron transfers are non-adiabatic (or diabatic) and are typical for long-range tunneling over several angstroms, as found in many proteins [7]. The kinetics of macromolecular electron tunneling are determined by semi-classical Marcus Theory, an application of Fermi's Golden Rule where the rate of charge transfer ($\mathrm{d}q/\mathrm{d}t$) between a donor and acceptor is controlled by a number of factors, including the redox potential difference (driving force) between these sites *and* the distance (r_{DA}) between them [7, 10–17]:

$$\frac{\mathrm{d}q\left(r_{\mathrm{DA}},\Delta\epsilon^0\right)}{\mathrm{d}t}\sim k_0'|H^0_{\mathrm{DA}}\exp\left(-0.5\beta r_{\mathrm{DA}}\right)|^2\exp\left(-\frac{\left[-\Delta\epsilon^0+\lambda\right]^2}{4\lambda k_{\mathrm{B}}T}\right), \qquad (1)$$

for electrons tunneling through an enzyme's electrically-insulating peptide matrix between donor and acceptor sites (figures 1(a) and (b)). Here, implicit Marcus (nuclear prefactor) terms are collapsed into the parameter k'_0 for brevity. Term ${H^0}_{\mathrm{DA}}$ gives the D-A coupling strength at the point of closest contact. The product $k'_0{H^\circ}_{\mathrm{DA}}{}^2 = k_0$ gives a uni-molecular rate constant for electron transfer ($\sim 10^{13}$ s^{-1}) at the minimum value of r_{DA}. Numerous changes to the tunneling decay constant, (β) and redox center reorganization energies (λ) may also be sampled over the course of protein evolution, marking additional, voltage-independent handles for ET rate control—and therefore catalytic control—in enzymes. Experimental confirmation of the Marcus description of charge transfer has been achieved through photochemical and electrochemical measurements of intramolecular electron transfer in various model systems, including *Pseudomonas aeruginosa* azurin [18–31], a variety of c-type cytochromes [18, 32–34] and members of the P450 cytochrome family [35], highlighting how only variation in r_{DA} permits the independent modulation of charge transfer rates, $\mathrm{d}q(r_{\mathrm{DA}}, \Delta\varepsilon^0)/\mathrm{d}t$, from the redox potential, $\Delta\varepsilon^0$. This ability to independently control charge transfer rates and reaction driving force provides nature with an extra level of control for tuning electron transfer kinetics and energetics, and therefore reactivity, over the course of protein evolution. A contour of Marcus-dependent tunneling in figure 1(c) summarizes this

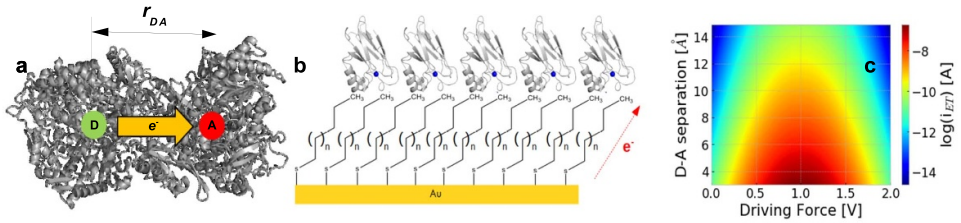

Figure 1. (a) Intramolecular electron transfer in proteins. The tunneling current is a partial function of donor(D)-acceptor(A) distance (r_{DA}) and the D-A redox potential difference (driving force). (b) Application of distance dependencies for regulating electron transfer. Incorporating self-assembling monolayers of thioalkyls on gold substrates allow for the imposition of tunneling barriers of defined widths, enabling electron transfer rates to be arbitrarily tuned at a single value of applied electrode potential. Barrier widths are generally controlled by using alkyl groups of varying methylenes (varying n). (c) Calculated one-electron Marcus contours of single-step, electron tunneling currents as a function of donor-acceptor distance and driving force (potential). The contours show it is possible to vary the tunneling current by orders of magnitude, independent of potential, by changing r_{DA}. Simulated at 293 K for $k_0 = 10^{13}$ s^{-1}, $\lambda = 1.0$ eV, $\beta = 1.4$ Å^{-1}, calculated using equation (1). Reprinted with permission from [39]. Copyright (2024) American Chemical Society.

phenomenon, demonstrating how a range of tunneling currents spanning several orders of magnitude may be realized for a single value of the driving force (potential), through variation of r_{DA}. As a result, it becomes apparent that nature enjoys several degrees of freedom for modulating tunneling current densities separately from redox potentials in proteins. This distinction marks a potential advantage for catalytic tuning in PEC systems that is disallowed by the constraints of dark electrochemistry, where changes to reaction driving forces (applied potential) necessarily alter reaction kinetics (current).

As in the case of proteins, electrochemical decoupling may, in principle, be achieved by exploiting the distance-dependence of electron tunneling. Specifically, the establishment of thin, electrically-insulating layers between the electrode substrate and some catalyst layer of interest may be used, with rate control at a given applied potential made possible by increasing or decreasing the insulator thickness (figures 1(b) and (c)). Changes to the barrier thickness grant control over the electrode-catalyst (donor-acceptor) tunneling distance, and consequently, the electron tunneling current. This approach for functional, current-potential decoupling has been borne-out in the field of molecular electronics, where previous studies on distance-dependent, electron tunneling through insulating barriers, such as alkyl layers on Au electrodes and metal oxide films, have demonstrated the possibility for controlling charge transfer to redox-active sites in this manner [16, 17, 36–38]. However, despite the significant body of work in this area, current-potential decoupling was not adopted as a general tool in the field of electrocatalysis. This omission is significant, as first-principles chemistry dictates that reactions will be under either thermodynamic or kinetic control. As a result, separate control over carrier kinetics and energetics may reasonably be expected to improve our ability to manipulate product branching ratios in electrochemical reactions.

3. Current-potential decoupling in inorganic systems and descriptive chemical analogies

Conventional dark voltammetry is conducted with an implicit understanding that current and potential cannot be independently controlled because the two mark co-dependent quantities, with variations in applied potential yielding corresponding changes in the current response of some given system of interest. The coupling between electrode current and potential is a relationship most commonly described using the Butler–Volmer formulation of interfacial electrode kinetics:

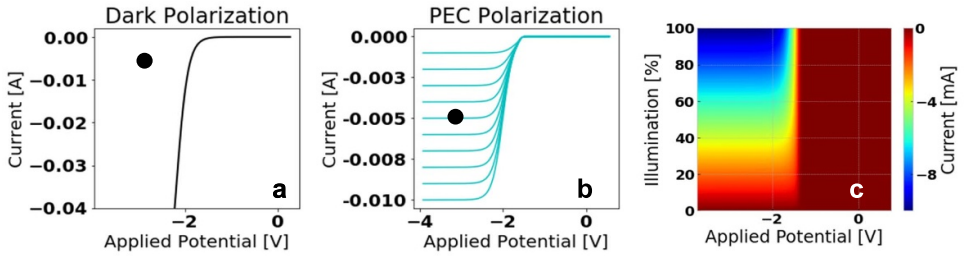

Figure 2. (a) Electrochemical polarization of a dark electrode/cell. Unlike with proteins, current and potential in dark electrochemical cells are coupled through one degree of freedom, with testable [*V,J*] coordinates only being those lying on the catalyst polarization curve (black line). Calculated using equation (1). The highly constrained polarization in the dark case means we cannot poise the system at the desired coordinate of [5 mA, 3 V] (black dot). (b) Simulated *J*–*V* response for PEC polarization. Here, independent control over applied voltage and current is achieved by biasing the photoelectrochemical cell driving electrocatalysis. Current may be separately controlled by varying the intensity of light incident of the PEC device. At high cell overpotentials, rates of electrocatalysis will be limited by the saturation current of the photoabsorber. With this PEC system, any polarization coordinate [*V,J*] in the region on or under the maximum current (−10 mA) polarization curve may now be tested. The result is that current and applied potential are functionally decoupled. Light intensity may be varied continuously, resulting in accessible polarization states that are described by the integral of the PEC polarization curve at maximum illumination. As a result, we can now arbitrarily poise the system at the desired coordinate [5 mA, 3 V] (black dot), and inspect how product distribution from CO_2 reduction (or another chemistry) changes as a result. (c) Contour mapping of this *J*–*V* decoupled, PEC system shows that current can be arbitrarily changed at a single voltage (by altering light illumination). Here, light acts as an additional degree of freedom for controlling current in analogy to the effects of distance-dependence in proteins, as shown in figure 1(c). (a)–(c) Reprinted with permission from [39]. Copyright (2024) American Chemical Society.

$$J(\eta) = J_0 \left[\exp\left(\frac{F\eta\alpha}{RT}\right) - \exp\left(-\frac{F\eta(1-\alpha)}{RT}\right) \right], \tag{2}$$

where η gives the electrode overpotential, α represents the symmetry factor, a term characterizing the transition state for electron transfer between donor and acceptor nuclear coordinates, and J_0 gives the equilibrium current density of forward and back reactions, defined at zero overpotential. Terms *F, R* and *T* represent Faraday's constant, the ideal gas constant, and system temperature, respectively. As a direct consequence of this, electrochemists treat the range of accessible operating conditions for an electrocatalyst as those combinations of current density and voltage (*J*–*V* coordinates, [*V,J*]) defining an electrocatalyst's polarization curve (figure 2(a)). As a result, it is generally not possible to vary current without changing a system's applied voltage.

While consideration of natural systems may be useful for illustrating the possibility of decoupling, attempting to tune current and applied potential independently, through step-wise changes in donor-acceptor distances in experimental systems, marks an inconvenient way of realizing decoupled electrocatalyst polarization. Such an approach would require that separate electrodes be fabricated for each donor-acceptor distance being tested. However, incorporation of light into electrochemical systems has been shown to make such explorations easier [39], with the independent control over current and voltage in a light-coupled apparatus yielding similar functional behavior as a system using distance-dependence as a mode of current-potential decoupling [39]. In general, the polarization response of semiconductor-liquid junctions incorporate aspects of both photovoltaics and dark electrocatalysts, with polarization curves that vary as both functions of potential and the light incident on the photoelectrode. Since incident light intensity may be varied by multiple means, such as placing a variable neutral density filter between the photoelectrode and light source, there exists a continuum of light-dependent, electrochemical response curves falling

beneath the maximum-illumination polarization curve, that may now be accessed (figure 2(b)). Here, our ability to vary electron energies by biasing a photoelectrode across a range of potentials (with a potentiostat), while independently limiting the total current—the rate of electron flow—by altering light intensity, yields a regime where current and applied potential are functionally decoupled. As a result, the expanded range of J–V coordinates in a decoupled system are now defined by the integral of the PEC polarization curve (with respect to applied potential) at maximum illumination. Now, electrocatalyst polarization assumes features akin to protein charge tunneling, with a continuum of current densities now accessible for a single value of applied potential/driving force (figure 2(c)).

This expansion of possible polarization states is expected to have real implications for steering electrocatalyst selectivity. In the case of CO_2 reduction, the well-documented observation of electrochemical hydrogen evolution (HER) kinetically out-competing CO_2 conversion at the high overpotentials where CO_2 reduction products also become energetically accessible [40], points to a useful role for decoupled polarization in mitigating adventitious HER. In particular, operating cathode catalysts in a low-current (kinetically limited), high overpotential (high energy) regime may enable CO_2 reduction with higher product selectivity. Notably, this option of selecting a cell/electrocatalyst polarization state of high overpotential and low current is generally precluded by dark voltammetry, where (non-mass transport limited) current scales as the exponent of applied potential. First-principles electrochemistry would suggest that operating electrocatalysts at decoupled current-potential coordinates lying beyond the dark polarization region (specifically in the low-current, high overpotential regime), may enable greater selectivity of CO_2RR over HER, while narrowing the distribution of reduced carbon products. Nascent efforts exploring decoupling in CO_2 conversion to syngas suggest this is indeed the case (figures 3(a)–(c)) [39], bolstering arguments for continuing these investigations on PEC decoupling in more complex catalytic systems. Explorations of Cu CO_2 reduction cathodes may prove especially illuminating, where the wide distribution of possible reduced-carbon products yielded during catalysis make matters of catalyst selectivity even more salient. It is critical to note the importance of using genuine semiconductor-liquid junctions for this purpose. The unique chemical behavior of such junctions, compared to buried junction or PV-electrolyzer (PV-E) devices, means that any changes in junction potential as a function of changing illumination state will not simply result in polarization states that are the same as those of a dark electrode/cell (EC). This is the case for PV-E and buried junction devices, where behavior of the illuminated PV-E cell is simply given by the overlap of the discrete PV and dark EC curves, and changes in illumination merely yield a cell or electrode polarization described by the dark EC curve [41, 42].

The possibility of arbitrarily controlling current and applied potentials is most easily understood by remembering that current density represents a flux that is influenced by more than a single parameter. Visualizing a stream of charge transiting through a conductive lattice at some potential ε, the energies associated with any of these charges ($q\varepsilon$), will be attenuated through collisions of conduction band electrons with the atoms comprising the conductor. The kinetic energy of these charges are dissipated in such collisions as heat—the genesis of the resistive properties giving rise to iR losses in an electrical circuit. The reduced kinetic energy of these charges, as their mean-free path is dampened by lattice collisions, reduces their average speed—and therefore their time-averaged flux—through the conductor. This ensemble charge flux is the measured current density, J, following the relation:

$$J(\epsilon) = nq\nu(\epsilon) \tag{3a}$$

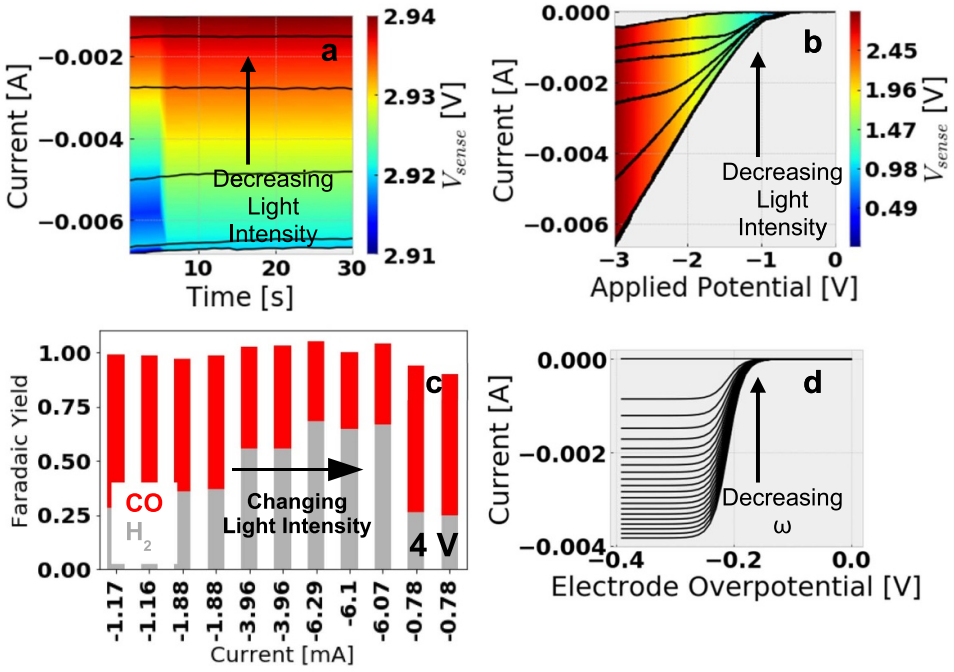

Figure 3. (a), (b) Monitoring PEC cell potentials as light is used to change current density. Bias is applied at the semiconductor-liquid interface, rather than a semiconductor back-contact. Monitoring a floating voltage contact at the liquid-semiconductor interface (V_{sense}) demonstrates the possibility of changing current magnitudes while stabilizing device operating potential, in a manner distinct from what is possible through PV-electrolyzer-type configurations. (c) Arbitrary current modulation in photoelectrochemical CO_2 reduction reveals that product distributions are found to vary along both voltage and current axes, as opposed to just changing as a function of voltage. (d) Simulated mass transport effects in a rotating-disk electrode, shown here for the case of 4-electron, O_2 reduction between 0 and 4000 rpm. Varied rotation rates (ω) give rise to similar behavior, with O_2 mass flux acting as a limit on charge propagation through the overall catalytic cycle for an arbitrary applied potential. (a)–(c) Reprinted with permission from [39]. Copyright (2024) American Chemical Society.

where n is the carrier density (m^{-3}), q gives the elementary charge (in coulombs), and $v(\varepsilon) = \nu_d + \nu_s$ is the carrier velocity (m s^{-1}), a sum of both drift (ν_d) and diffusion (ν_s) components. A simplified description of the carrier velocity's potential dependence is found by considering the carrier drift velocity (ν_d):

$$\nu_d(\epsilon) = \mu\vec{E}(\epsilon). \tag{3b}$$

Here, μ gives the carrier mobility for a material. E is the electric field strength, an implicit function of the potential, ε, whose modulation is found to influence carrier drift velocity.

As implied by equation (3*a*), we can also imagine manipulating this flux by simply changing n rather than v. In the case of metals, the significant occupancy of conduction band states at room temperature yields a high carrier concentration that remains essentially constant under ambient conditions, making it virtually impossible to modulate J through changes in n, and forming the basis for why electrochemical polarization at metal and carbon electrodes is facilitated through applied potential modulation alone. However, semiconducting materials are unique in that their carrier concentrations are responsive to incident light absorption, opening a route for manipulating carrier fluxes through changes in carrier concentration, rather than the potential-dependent parameter v, as shown by equation (4*a*):

$$n \propto \gamma - r_{\text{defect}} - r_{\text{rad}} - r_{\text{Auger}}, \tag{4a}$$

where γ is the carrier generation rate, while r_{defect}, r_{rad} and r_{Auger} refer to charge recombination rates due to defects, radiative recombination, and Auger recombination, respectively. The light dependence of n in a doped semiconductor arises from γ:

$$\gamma = \int_{x_1}^{x_2} \int_{\lambda_1}^{\lambda_2} I_0(\lambda)\,\alpha(\lambda)\,e^{-x\alpha(\lambda)}\mathrm{d}\lambda\mathrm{d}x, \tag{4b}$$

where I_0 gives the spectrum-dependent incident photon flux, $\alpha(\lambda)$ gives the light absorption coefficient as a function of wavelength (λ), and x is the depth from the illuminated semiconductor surface. Integration across all incident wavelengths, over all depths in the semiconductor from the illuminated surface, give the total carrier generation rate. As a result, light absorption can be seen to provide a secondary mode for controlling carrier flux—by altering n rather than v–in a manner that displays no explicit potential dependence.

This proposition of controlling carrier fluxes by manipulating carrier concentrations—rather than by parameters (such as potential) that influence mean carrier velocities—should not be too foreign to a chemist, because it is largely a restatement of effects already well-understood in physical chemistry. In electrochemistry, reaction fluxes under mass transport control represent the product of both diffusive rate constants of a species and the species concentration, as captured by the Fickian laws [43, 44]. Furthermore, it is well understood just how pronounced the effects of mass transport may be on steering the course of electrochemical reactivity [45]. As a result, in the case of mass-transport controlled reactions, electron flows may be regulated by controlling substrate delivery to an active site by changing either the substrate concentration or parameters that impact rates of diffusive transport (by changing electrolyte viscosity, for example), neither of which have voltage dependencies. The net effects are outcomes with close functional relationships to those posited by current-potential decoupling—specifically, using additional degrees of freedom (here, changes to substrate mixing, diffusion rates or substrate concentration) as methods for enabling arbitrary current selection for a given applied potential. This point is underscored by considering the qualitative similarity between polarization curves generated through Levich analysis [44, 46] using a rotating disk electrode and the light-limited curves generated using a PEC device to independently vary current and applied potential. In the former case, changes in electrode rotation rate (ω) will cause current flows to vary significantly, even at a single value of the applied electrode potential, with potential consequences for reaction selectivity (figure 3(d)). The latter instance, however, offers a way to achieve such functionality generally, for any reaction of choice, rather than the particular case of mass-transport-limited systems.

4. Unifying decoupled protein electron transfer and artificial electrocatalysis

The option of independently controlling carrier kinetics and carrier energetics should prompt a closer consideration of how redox-active proteins regulate their high catalytic specificities, with an eye on translating the physical principles by which these biochemical systems operate, into the design of artificial catalysts. The observation that nature uses a relatively small suite of redox cofactors to access a wide range of redox-dependent transformations becomes less surprising, when stopping to realize the various ways by which reactivities of such active sites may be tuned to accommodate a wide range of chemistries. As Marcus Theory suggests, this may be achieved, in part, by regulating inter-site electron

transfers independently of the potential through which the charge carrier travels, by positioning these redox-active motifs at unique distances in different proteins. Indeed, work on cytochrome P450s have shown that regulation of electron transfer rates alone—without changes in inter-site redox potential—are enough to impact the observation of photochemically-generated redox intermediates [47–49] and the product distributions resulting from electrochemical enzyme turnover [35].

Given that the range of testable [*V,J*] coordinates is infinitely greater in the decoupled case than it is for a conventional dark electrochemical experiment, testing a broad range of polarization conditions for a given catalyst may quickly become a time-prohibitive exercise, with product accumulation and measurement taking anywhere from minutes to hours for every polarization coordinate tested. As a result, the task of testing different polarization conditions in a decoupled system, depending on the catalyst or step-resolution of the experiment, may range from time-consuming to intractable. However, previous advancements in our ability to quantitatively describe charge tunneling in biological systems may provide a useful route for circumventing this issue. In dynamic systems such as complex macromolecules, realistic determination of charge transfer rates must account for the time-averaged fluctuations in distance between two redox sites in a dynamic protein structure that may be rapidly sampling different conformations. As a result, the overall rate term becomes a weighted sum dependent on the electronic coupling strength (H_{DA}) of various paths available for charge transfer between donor and acceptor sites in these systems, with charge transfer rates being proportional to ${H_{DA}}^2$ [13, 15, 50–53]. Here we find ourselves at an advantage, as computational solutions for handling these complexities have already been developed. In particular, the pioneering computational methods of Beratan and Onuchic have facilitated the path-dependent calculation of inter-site electron transfers in proteins with solved structures, permitting the explicit determination of otherwise hard-to-know electron transfer rates in proteins [54–58]. Beratan and Onuchic's approach—codified by Balabin in the *PATHWAYS* algorithm—solves the problem of how to determine possible competing routes for electron transfer by calculating the electron coupling between donor and acceptor for every possible charge transfer path. Overall couplings are calculated by decomposing transfer paths into a series of discrete steps comprised of charge hopping or tunneling through covalent bonds, hydrogen bonds and through-space jumps [58]:

$$H_{DA} \propto \prod_i w_i^c \prod_j w_j^h \prod_k w_k^s. \tag{5}$$

The method embodied in equation (5) determines H_{DA} of a given pathway, expressed as the product of a series of individual covalent bond (w^c), hydrogen bond (w^h), and through-space (w^s) electronic couplings that occur between adjacent sites for electron hopping between an arbitrarily located donor and acceptor.

Such capabilities, paired with an ability to determine relevant redox potentials using established analytical methods such as spectroelectrochemical titration, provide chemists with the tools necessary for determining the effective current-potential coordinate at which a given enzyme operates. Application of such information to decoupled regulation of charge transfer could then help identify promising [*V,J*] coordinates for a related inorganic material, where catalysis may be optimal. For example, it is conceivable that MoS_2 and related 2D materials may be competent for CO_2 reduction in aqueous media. However, efforts to date have only succeeded in using these materials in proton reduction [59–66] and CO_2 reduction in non-aqueous media [67, 68], with only marginal activities being observed under aqueous conditions [69]. This is despite the perfect fidelity with which molybdo-sulfur and tungsto-sulfur formate

dehydrogenase enzymes interconvert CO_2 and formate. However, incorporation of decoupled polarization may provide us with an expanded set of conditions under which we can test such materials, and the knowledge of the [*V,J*] operating points characterizing a redox enzyme may help us reduce the time needed to explore this expanded space of polarization conditions in a decoupled PEC device. Conversely, pursuing this line of scientific inquiry may also reveal fundamental relationships between current-potential coordinates characterizing a redox enzyme and the chemical transformations it can facilitate. The possibility of uncovering such correlations is suggested by recent findings, where utilization of decoupling revealed the existence of a smooth relation between [*V,J*] coordinate (rather than voltage alone as is commonly assumed) and product ratios in electrochemical CO_2 reduction [39].

5. Outlook

Independent manipulation of current and applied potential as handles for steering electrochemical reactions should motivate a reexamination of the predominant approaches to biomimetic electrocatalysis. While biophysical design emphases and synthetic bioinorganic approaches are often spoken of interchangeably, the distinctions between the two are critical, and are perhaps best highlighted via analogy: both a bird and a helicopter can fly, though the physical resemblance between the two is weak. A narrow focus on building flying machines by assuming they must look like a bird would have likely precluded the helicopter's invention. However, a general comprehension of Bernoulli's physical Principle of Lift opens up the possibility of using a narrow, rotary blade instead of a broad, wing-like structure for flight. The comparison demonstrates how aesthetic dissimilarity between two structures may nevertheless yield a functional convergence, so long as they operate under the same physical principle. This highlights the key difference between mimicking natural catalytic schemes using biophysical vs synthetic bioinorganic approaches. In the latter case, efforts to replicate enzyme chemistries have placed an overwhelming emphasis on the assumed essence of structure-function correlations, a fact exemplified by the synthesis of molecular complexes that resemble protein active sites but rarely yield reactivities comparable to the corresponding enzyme. However, recent findings suggest that a worthy aim of catalyst development may be to incorporate more of the biophysical design paradigm alongside synthetic bioinorganic treatments, through an increased focus on emulating the underlying physics of enzyme functioning, rather than operating under assumptions that structural similarities to protein active sites alone will be enough. In the case of reproducing nature's regulation of electron transport in enzyme catalysis, electrochemical decoupling may provide an important step forward, as the field of electrocatalysis advances towards fully functional biomimicry.

Data availability statement

No new data were created or analysed in this study.

Acknowledgments

This work was supported by the Liquid Sunlight Alliance a DOE Energy Innovation Hub, supported through the Office of Science of the U.S. Department of Energy under Award Number DE-SC0021266.

Conflict of interest

The author declares no competing interests.

ORCID iD

Peter Agbo https://orcid.org/0000-0003-3066-4791

References

[1] Kanady J S, Tsui E Y, Day M W and Agapie T 2011 A synthetic model of the Mn_3Ca subsite of the oxygen-evolving complex in photosystem II *Science* **333** 733–6
[2] Kanady J S, Lin P-H, Carsch K M, Nielsen R J, Takase M K, Goddard W A and Agapie T 2014 Toward models for the full oxygen-evolving complex of photosystem II by ligand coordination to lower the symmetry of the Mn_3CaO_4 cubane: demonstration that electronic effects facilitate binding of a fifth metal *J. Am. Chem. Soc.* **136** 14373–6
[3] Hlavica P 2004 Models and mechanisms of O-O bond activation by cytochrome P450 *Eur. J. Biochem.* **271** 4335–60
[4] Sommer D J, Vaughn M D and Ghirlanda G 2014 Protein secondary-shell interactions enhance the photoinduced hydrogen production of cobalt protoporphyrin IX *Chem. Commun.* **50** 15852–5
[5] Iost R M, Venkatkarthick R, Nascimento S Q, Lima F H B and Crespilho F N 2024 Hydrogen bioelectrogeneration with pH-resilient and oxygen-tolerant cobalt apoenzyme-saccharide *Chem. Commun.* **60** 2509–11
[6] Kuriyan J 2013 *The Molecules of Life: Physical and Chemical Principles* (Garland Science, Taylor & Francis Group)
[7] Marcus R A and Sutin N 1985 Electron transfers in chemistry and biology *Biochim. Biophys. Acta* **811** 265–322
[8] Wiechen M, Najafpour M M, Allakhverdiev S I and Spiccia L 2014 Water oxidation catalysis by manganese oxides: learning from evolution *Energy Environ. Sci.* **7** 2203–12
[9] Umena Y, Kawakami K, Shen J-R and Kamiya N 2011 Crystal structure of oxygen-evolving photosystem II at a resolution of 1.9 Å *Nature* **473** 55–60
[10] Winkler J R, Di Bilio A, Farrow N A, Richards J H and Gray H B 1999 Electron tunneling in biological molecules *Pure Appl. Chem.* **71** 1753–64
[11] Gray H B and Winkler J R 2005 Long-range electron transfer *Proc. Natl Acad. Sci.* **102** 3534–9
[12] Gray H B and Winkler J R 2003 Electron tunneling through proteins *Q. Rev. Biophys.* **36** 341–72
[13] Warren J J, Ener M E, Vlček A Jr, Winkler J R and Gray H B 2012 Electron hopping through proteins *Coord. Chem. Rev.* **256** 2478–87
[14] Saen-Oon S, Lucas M F and Guallar V 2013 Electron transfer in proteins: theory, applications and future perspectives *Phys. Chem. Chem. Phys.* **15** 15271
[15] Voityuk A A 2011 Long-range electron transfer in biomolecules. Tunneling or hopping? *J. Phys. Chem.* B **115** 12202–7
[16] Finklea H O and Hanshew D D 1992 Electron-transfer kinetics in organized thiol monolayers with attached pentaammine(pyridine)ruthenium redox centers *J. Am. Chem. Soc.* **114** 3173–81
[17] Smalley J F, Feldberg S W, Chidsey C E D, Linford M R, Newton M D and Liu Y-P 1995 The kinetics of electron transfer through ferrocene-terminated alkanethiol monolayers on gold *J. Phys. Chem.* **99** 13141–9
[18] Cummins D and Gray H B 1977 Electron-transfer protein reactivities. Kinetic studies of the oxidation of horse heart cytochrome c, Chromatium vinosum high potential iron-sulfur protein, Pseudomonas aeruginosa azurin, bean plastocyanin, and Rhus vernicifera stellacyanin by pentaammminepyridineruthenium (III) *J. Am. Chem. Soc.* **99** 5158–67
[19] Bordi F, Prato M, Cavalleri O, Cametti C, Canepa M and Gliozzi A 2004 Azurin self-assembled monolayers characterized by coupling electrical impedance spectroscopy and spectroscopic ellipsometry *J. Phys. Chem.* A **108** 20263–72
[20] Farver O, Skov L K, Young S, Bonander N, Karlsson B G, Vänngaard T and Pecht I 1997 Aromatic residues may enhance intramolecular electron transfer in azurin *J. Am. Chem. Soc.* **119** 5453–4
[21] Lancaster K M, Farver O, Wherland S, Crane E J, Richards J H, Pecht I and Gray H B 2011 Electron transfer reactivity of type zero Pseudomonas aeruginosa azurin *J. Am. Chem. Soc.* **133** 4865–73
[22] Farver O and Pecht I 1992 Long range intramolecular electron transfer in azurins *J. Am. Chem. Soc.* **114** 5764–7

[23] Farver O, Lu Y, Ang M C and Pecht I 1999 Enhanced rate of intramolecular electron transfer in an engineered purple CuA azurin *Proc. Natl Acad. Sci.* **96** 899–902
[24] Gray H B and Winkler J R 2010 Electron flow through metalloproteins *Biochim. Biophys. Acta* **1797** 1563–72
[25] Yokoyama K, Leigh B S, Sheng Y, Niki K, Nakamura N, Ohno H, Winkler J R, Gray H B and Richards J H 2008 Electron tunneling through Pseudomonas aeruginosa azurins on SAM gold electrodes *Inorg. Chim. Acta* **361** 1095–9
[26] Fujita K, Nakamura N, Ohno H, Leigh B S, Niki K, Gray H B and Richards J H 2004 Mimicking protein−protein electron transfer: voltammetry of Pseudomonas aeruginosa azurin and the thermus thermophilus CuA domain at ω-derivatized self-assembled-monolayer gold electrodes *J. Am. Chem. Soc.* **126** 13954–61
[27] Shih C *et al* 2008 Tryptophan-accelerated electron flow through proteins *Science* **320** 1760–2
[28] Sepunaru L, Pecht I, Sheves M and Cahen D 2011 Solid-state electron transport across azurin: from a temperature-independent to a temperature-activated mechanism *J. Am. Chem. Soc.* **133** 2421–3
[29] Farver O, Marshall N M, Wherland S, Lu Y and Pecht I 2013 Designed azurins show lower reorganization free energies for intraprotein electron transfer *Proc. Natl Acad. Sci.* **110** 10536–40
[30] Crane B R, Di Bilio A J, Winkler J R and Gray H B 2001 Electron tunneling in single crystals of Pseudomonas aeruginosa azurins *J. Am. Chem. Soc.* **123** 11623–31
[31] Khoshtariya D E, Dolidze T D, Shushanyan M, Davis K L, Waldeck D H and van E R 2010 Fundamental signatures of short- and long-range electron transfer for the blue copper protein azurin at Au/SAM junctions *Proc. Natl Acad. Sci.* **107** 2757–62
[32] Gray H B and Winkler J R 2009 Electron flow through proteins *Chem. Phys. Lett.* **483** 1–9
[33] Kuznetsov B A, Byzova N A and Shumakovich G P 1994 The effect of the orientation of cytochrome c molecules covalently attached to the electrode surface upon their electrochemical activity *J. Electroanal. Chem.* **371** 85–92
[34] Alvarez-Paggi D, Meister W, Kuhlmann U, Weidinger I, Tenger K, Zimányi L, Rákhely G, Hildebrandt P and Murgida D H 2013 Disentangling electron tunneling and protein dynamics of cytochrome c through a rationally designed surface mutation *J. Phys. Chem.* B **117** 6061–8
[35] van der Felt C *et al* 2011 Electron-transfer rates govern product distribution in electrochemically-driven P450-catalyzed dioxygen reduction *J. Inorg. Biochem.* **105** 1350–3
[36] Devaraj N K, Decreau R A, Ebina W, Collman J P and Chidsey C E D 2006 Rate of interfacial electron transfer through the 1,2,3-triazole linkage *J. Phys. Chem.* B **110** 15955–62
[37] Neuhausen A B, Hosseini A, Sulpizio J A, Chidsey C E D and Goldhaber-Gordon D 2012 Molecular junctions of self-assembled monolayers with conducting polymer contacts *ACS Nano* **6** 9920–31
[38] Chidsey C E D 1991 Free energy and temperature dependence of electron transfer at the metal-electrolyte interface *Science* **251** 919–22
[39] Agbo P 2024 An expansion of polarization control using semiconductor–liquid junctions *J. Phys. Chem. Lett.* **15** 1135–42
[40] Huan T N *et al* 2019 Low-cost high-efficiency system for solar-driven conversion of CO_2 to hydrocarbons *Proc. Natl Acad. Sci.* **116** 9735–40
[41] Walter M G, Warren E L, McKone J R, Boettcher S W, Mi Q, Santori E A and Lewis N S 2010 Solar water splitting cells *Chem. Rev.* **110** 6446–73
[42] Agbo P 2020 *J*–*V* decoupling: independent control over current and potential in electrocatalysis *J. Phys. Chem.* C **124** 28387–94
[43] Bockris J O, Reddy A K N and Gamboa-Aldeco M 2000 *Modern Electrochemistry* (Springer)
[44] Bard A J and Faulkner L R 2001 *Electrochemical Methods: Fundamentals and Applications* (Wiley)
[45] Watkins N B, Schiffer Z J, Lai Y, Musgrave C B I, Atwater H A, Goddard W A I, Agapie T, Peters J C and Gregoire J M 2023 Hydrodynamics change tafel slopes in electrochemical CO_2 reduction on copper *ACS Energy Lett.* **8** 2185–92
[46] Wang J, Zhao C-X, Liu J-N, Ren D, Li B-Q, Huang J-Q and Zhang Q 2021 Quantitative kinetic analysis on oxygen reduction reaction: a perspective *Nano Mater. Sci.* **3** 313–8
[47] Ener M E, Gray H B and Winkler J R 2017 Hole hopping through tryptophan in cytochrome P450 *Biochemistry* **56** 3531–8
[48] Krest C M, Onderko E L, Yosca T H, Calixto J C, Karp R F, Livada J, Rittle J and Green M T 2013 Reactive intermediates in cytochrome P450 catalysis* *J. Biol. Chem.* **288** 17074–81
[49] Ener M E, Lee Y-T, Winkler J R, Gray H B and Cheruzel L 2010 Photooxidation of cytochrome P450-BM3 *Proc. Natl Acad. Sci.* **107** 18783–6
[50] Ricks A B, Solomon G C, Colvin M T, Scott A M, Chen K, Ratner M A and Wasielewski M R 2010 Controlling electron transfer in donor−bridge−acceptor molecules using cross-conjugated bridges *J. Am. Chem. Soc.* **132** 15427–34
[51] Walther M E and Wenger O S 2011 Hole tunneling and hopping in a Ru(bpy)32+-phenothiazine dyad with a bridge derived from oligo-p-phenylene *Inorg. Chem.* **50** 10901–7

[52] Wenger O S 2010 How donor−bridge−acceptor energetics influence electron tunneling dynamics and their distance dependences *Acc. Chem. Res.* **44** 25–35
[53] Warren J J, Winkler J R and Gray H B 2013 Hopping maps for photosynthetic reaction centers *Coord. Chem. Rev.* **257** 165–70
[54] Beratan D N, Betts J N and Onuchic J N 1992 Tunneling pathway and redox-state-dependent electronic couplings at nearly fixed distance in electron transfer proteins *J. Phys. Chem.* **96** 2852–5
[55] Beratan D N, Betts J N and Onuchic J N 1991 Protein electron transfer rates set by the bridging secondary and tertiary structure *Science* **252** 1285–8
[56] Balabin I A, Beratan D N and Skourtis S S 2008 Persistence of structure over fluctuations in biological electron-transfer reactions *Phys. Rev. Lett.* **101** 158102
[57] Onuchic J N, Beratan D N, Winkler J R and Gray H B 1992 Pathway analysis of protein electron-transfer reactions *Annu. Rev. Biophys. Biomol. Struct.* **21** 349–77
[58] Balabin I A, Hu X and Beratan D N 2012 Exploring biological electron transfer pathway dynamics with the pathways plugin for VMD *J. Comput. Chem.* **33** 906–10
[59] Lukowski M A, Daniel A S, Meng F, Forticaux A, Li L and Jin S 2013 Enhanced hydrogen evolution catalysis from chemically exfoliated metallic MoS_2 nanosheets *J. Am. Chem. Soc.* **135** 10274–7
[60] Laursen A B, Pedersen T, Malacrida P, Seger B, Hansen O, Vesborg P C K and Chorkendorff I 2013 MoS_2—an integrated protective and active layer on n+p-Si for solar H_2 evolution *Phys. Chem. Chem. Phys.* **15** 20000–4
[61] Kong D, Wang H, Cha J J, Pasta M, Koski K J, Yao J and Cui Y 2013 Synthesis of MoS_2 and $MoSe_2$ films with vertically aligned layers *Nano Lett.* **13** 1341–7
[62] Xue N and Diao P 2017 Composite of few-layered MoS_2 grown on carbon black: tuning the ratio of terminal to total sulfur in MoS_2 for hydrogen evolution reaction *J. Phys. Chem.* C **121** 14413–25
[63] Chang K and Chen W 2011 *In situ* synthesis of MoS_2/graphene nanosheet composites with extraordinarily high electrochemical performance for lithium ion batteries *Chem. Commun.* **47** 4252–4
[64] King L A, Hellstern T R, Park J, Sinclair R and Jaramillo T F 2017 Highly stable molybdenum disulfide protected silicon photocathodes for photoelectrochemical water splitting *ACS Appl. Mater. Interfaces* **9** 36792–8
[65] Jaramillo T F, Jorgensen K P, Bonde J, Nielsen J H, Horch S and Chorkendorff I 2007 Identification of active edge sites for electrochemical H_2 evolution from MoS_2 nanocatalysts *Science* **317** 100–2
[66] Wu Z, Fang B, Wang Z, Wang C, Liu Z, Liu F, Wang W, Alfantazi A, Wang D and Wilkinson D P 2013 MoS_2 nanosheets: a designed structure with high active site density for the hydrogen evolution reaction *ACS Catal.* **3** 2101–7
[67] Abbasi P, Asadi M, Liu C, Sharifi-Asl S, Sayahpour B, Behranginia A, Zapol P, Shahbazian-Yassar R, Curtiss L A and Salehi-Khojin A 2017 Tailoring the edge structure of molybdenum disulfide toward electrocatalytic reduction of carbon dioxide *ACS Nano* **11** 453–60
[68] Asadi M *et al* 2016 Nanostructured transition metal dichalcogenide electrocatalysts for CO_2 reduction in ionic liquid *Science* **353** 467–70
[69] Francis S A *et al* 2018 Reduction of Aqueous CO_2 to 1-propanol at MoS_2 electrodes *Chem. Mater.* **30** 4902–8